5.0 NEXT-GENERATION INSTRUMENT CONCEPTS

Studies of the potential next-generation earth radiation budget instrument, PERSEPHONE, as described in Chapter 2.0, require the use of a radiative model of the CERES and/or modified CERES telescope. The first task of the current effort was to develop such a model which is flexible enough to perform the required studies. Repeating the research objectives of this thesis topic, the first goal is to determine the maximum number of detectors that can be placed in the current CERES telescope without the loss of Optical Point Spread Function (OPSF) quality. The other principal objective is to investigate the possibility of using hyperbolic mirrors in place of the current spherical mirrors in order to maximize the number of channels that can be fitted into the current CERES envelope, thus maximizing the science data return. Descriptions of these studies, and their results are presented in this chapter.

5.1 Development of the radiative model of the CERES optics

Members of the Thermal Radiation Group have developed several radiative models of the CERES and ERBE telescopes. Meekins [1990] completed a Monte-Carlo-based numerical model to study the optical and radiative characteristics of the ERBE scanning radiometer. Bongiovi [1993] later modified Meekins' code, adding baffles in order to

model the CERES instrument. Bongiovi's code consists of 16,632 lines of commented FORTRAN code, and is specific to the CERES geometry. Modification of this code to conduct the study at hand would be a formidable task. Instead, a new radiative model was developed using a tool which is being developed by Félix Nevárez, a doctoral student in the Thermal Radiation Group. This tool consists of a C^{++} class library which can represent quadric surfaces, such as cylinders, spheres, planes, and cones with specified surface absorptivity and specularity ratio. The radiative model of an instrument can be developed by modeling each interior instrument surface using one of the library-defined surfaces with appropriate dimensions, and stacking these surfaces to model the entire instrument. After the complete geometry is described, a Monte-Carlo engine module is called, and a user-specified number of energy bundles is directed through the instrument. The paths of these energy bundles are determined by following the rules of the Monte-Carlo ray-trace method as it applies to radiation heat transfer. The output from the execution of this C code is a file of the distribution of energy bundles arriving on a surface of interest.

5.1.1 Modeling the CERES geometry

In the present instrument study, the surface of interest is the plane which would contain an array of thermistor bolometer detectors, located beneath the precision aperture pictured in Figure 5.1 (b). Figure 5.1 (a) demonstrates how the CERES telescope is broken down into 46 basic surfaces. The numbering scheme corresponds to the numbering used in the code provided in Appendix C. Note that with the use of this new tool, the author needed only to write 616 lines of commented C code which calls the C^{++} library functions, and 224 lines of FORTRAN code for post-processing the output files, for a total of 840 lines of code. When compared to Bongiovi's 16,632 lines of FORTRAN required to achieve the same task, this new code proves to be a remarkable tool in radiometric instrument design.

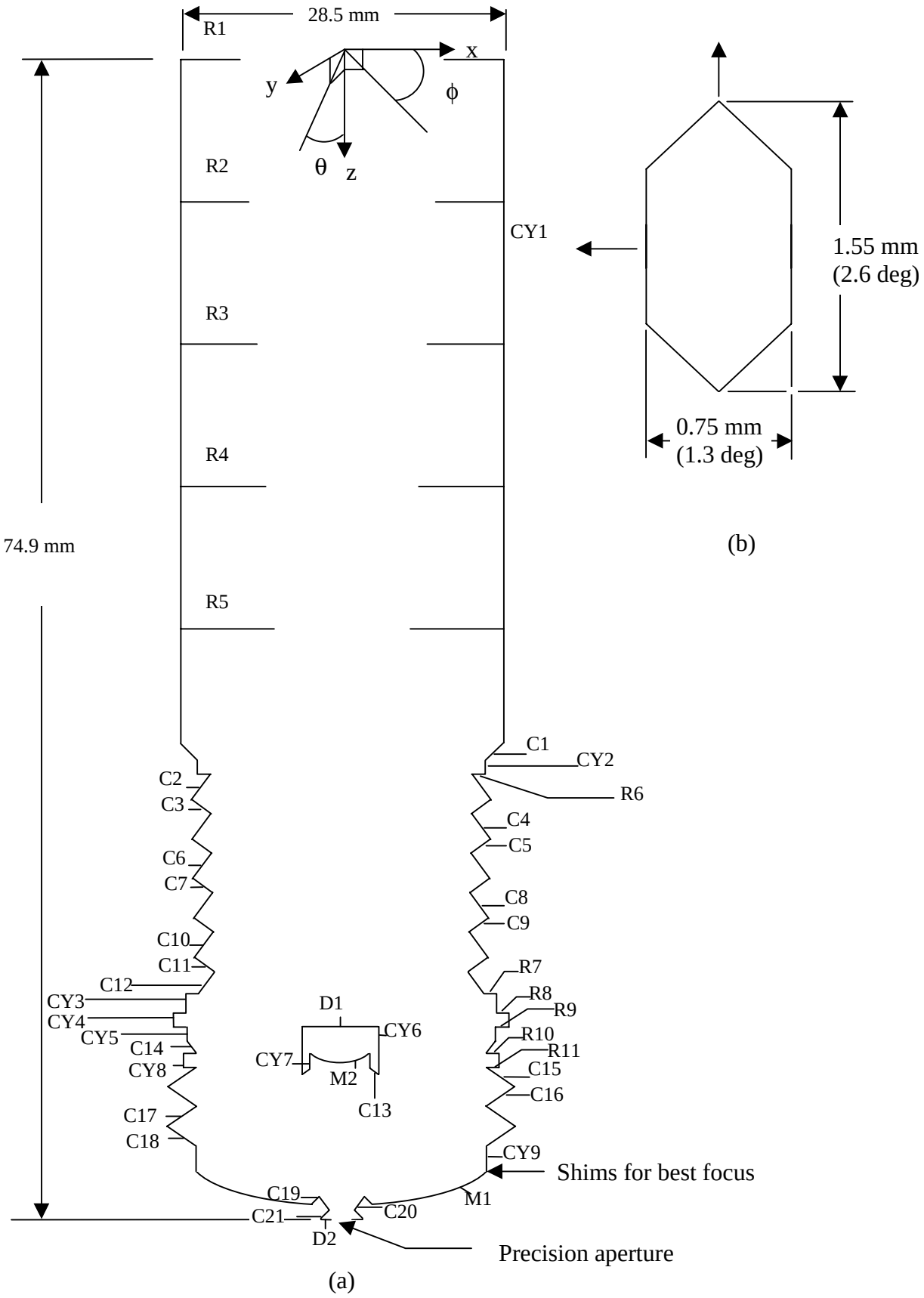

Figure 5.1 (a) Illustration of components of CERES geometry, excluding the "spider legs" which support the secondary mirror (not drawn to scale), and (b) the precision aperture in CERES telescope.

In addition to the ease of performing radiometric analyses, this new ray-trace environment is equipped with a useful graphical user interface. After entering the telescope geometry, it can be viewed by specifying all of the surfaces as diffuse and firing rays into the telescope. Figure 5.2 shows the CERES telescope with the primary mirror removed, as produced by this graphical user interface.

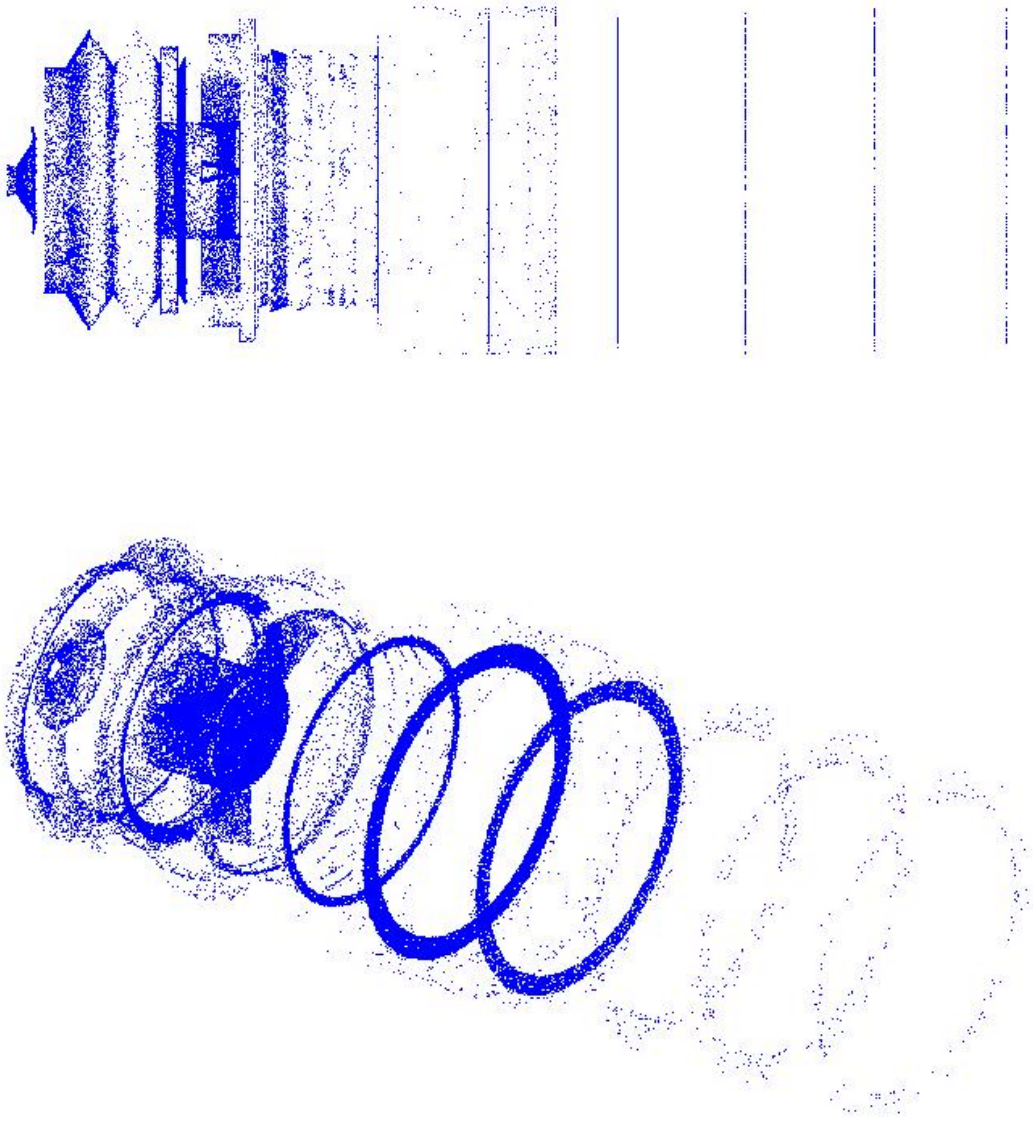

Figure 5.2 CERES telescope geometry, as produced by graphical user interface of the new ray-trace environment.

5.1.2 Addition of shims for blur circle minimization

As described in Chapter 3.0, the presence of spherical aberration in an optical system causes the spot size at the point of "best focus" to be finite. This spot of finite diameter is called the blur circle. It is desired that the location of the minimum blur circle occur at the plane containing the precision aperture so that the edges of the Optical Point Spread Function demonstrate the steepest drop-off possible (i.e. approach a "top-hat" response). The location of the "best focus" is very sensitive to the distance between the primary and secondary mirrors. Upon placing the parts between these mirrors, tolerance stack-up occurs so that the location of the minimum blur circle will likely not occur at the plane containing the precision aperture. The spacing between the mirrors is thus increased by the addition of very thin shims until the blur circle is a minimum at the precision aperture. This addition of shims was simulated using the computer model of the CERES telescope. The distance between the mirrors was gradually increased, and a scattergram representing the blur circle was plotted until the distance providing the minimum blur circle was found. The change in the image at the focal plane due to slight changes in the primary-to-secondary mirror spacing is illustrated in Figure 5.3. The quantity δ refers to the total thickness of the shims added. When δ = 0.28 mm, the minimum blur circle is obtained, as illustrated in Figure 5.3 (b). Note that the structure which supports the secondary mirror, the "spider", is imaged in the defocused images shown in Figures 5.3 (a) and (c).

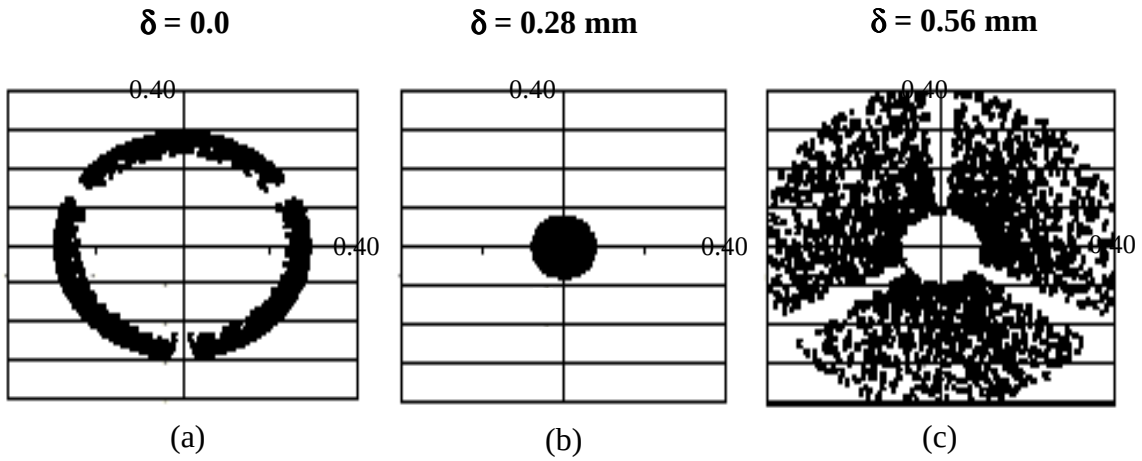

Figure 5.3 Illustration of change in the images at the precision aperture for different shim thicknesses, where δ is the shift due to the addition of shims (dimensions in mm). (a) Defocused image, (b) image at best focus where the blur circle diameter is a minimum, and (c) defocused image.

5.2 Capabilities of the current CERES instrument

5.2.1 Determination of the Optical Point Spread Function of the current CERES instrument

The OPSF (Optical Point Spread Function) of an instrument shows how collimated energy entering from various angles is transmitted through the instrument. The OPSF has previously been determined for the CERES telescope with only a single aperture using Bongiovi's model [Priestley, 1997]. This OPSF exhibits attenuation at the edges of the field due to the finite blur circle. If the blur circle were infinitely small, as in an ideal optical system, this edge attenuation would be absent from the OPSF. This ideal OPSF would be perfectly flat across the aperture area, and would drop immediately to zero beyond the edges. Instead, attenuation occurs before the physical edge of the field stop is reached, and radiation arrives at the detector beyond the projection of the area of the field stop on the detector. A complete description of the significance of the blur circle is presented by Priestley [1997].

Equivalence is assumed in the determination of the OPSF of the CERES telescope. This assumption implies that regardless of the point at which a given amount of energy arrives at a thermistor bolometer detector, the response of the detector is the same.

In order to determine the OPSF over more than one aperture using the new radiative model, collimated radiation was allowed to arrive at angles θ, ϕ (see Figure 5.1 (a)) and traced through the instrument. The output file for a given combination of angles consists of the x, y coordinates of all energy bundles arriving at the plane containing the precision aperture. In order to determine how much of this arriving energy enters one of the precision apertures, each output file must be opened and read, line by line. If the coordinates of a line of output fall within the area defined by of one of the precision apertures, then an energy bundle will reach the detector below, and a counter for that aperture is incremented. After all lines of all output files have been read, the results are the number of energy bundles arriving to each detector for each set of input angles θ, ϕ. This is the information needed to construct the OPSF of the instrument. The FORTRAN

code used to perform this post processing is provided in Appendix C. Figures 5.4 and 5.5 show the resulting OPSF of the current CERES instrument with five (5) apertures and two (2) apertures, respectively. Section 5.2.3 provides an interpretation of these figures.

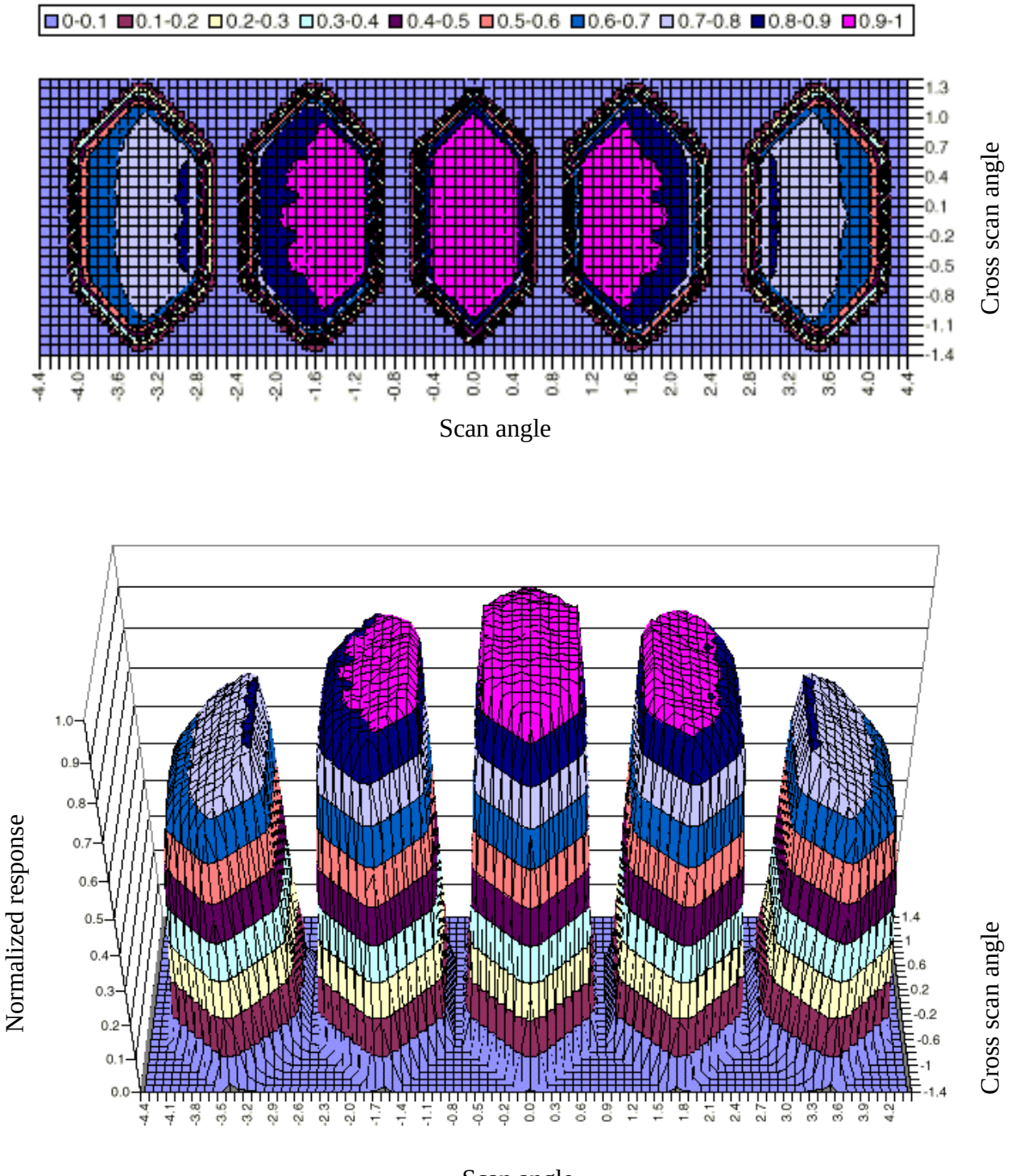

Figure 5.4 OPSF for the current CERES telescope (minus the primary mirror insert) with five (5) precision apertures.

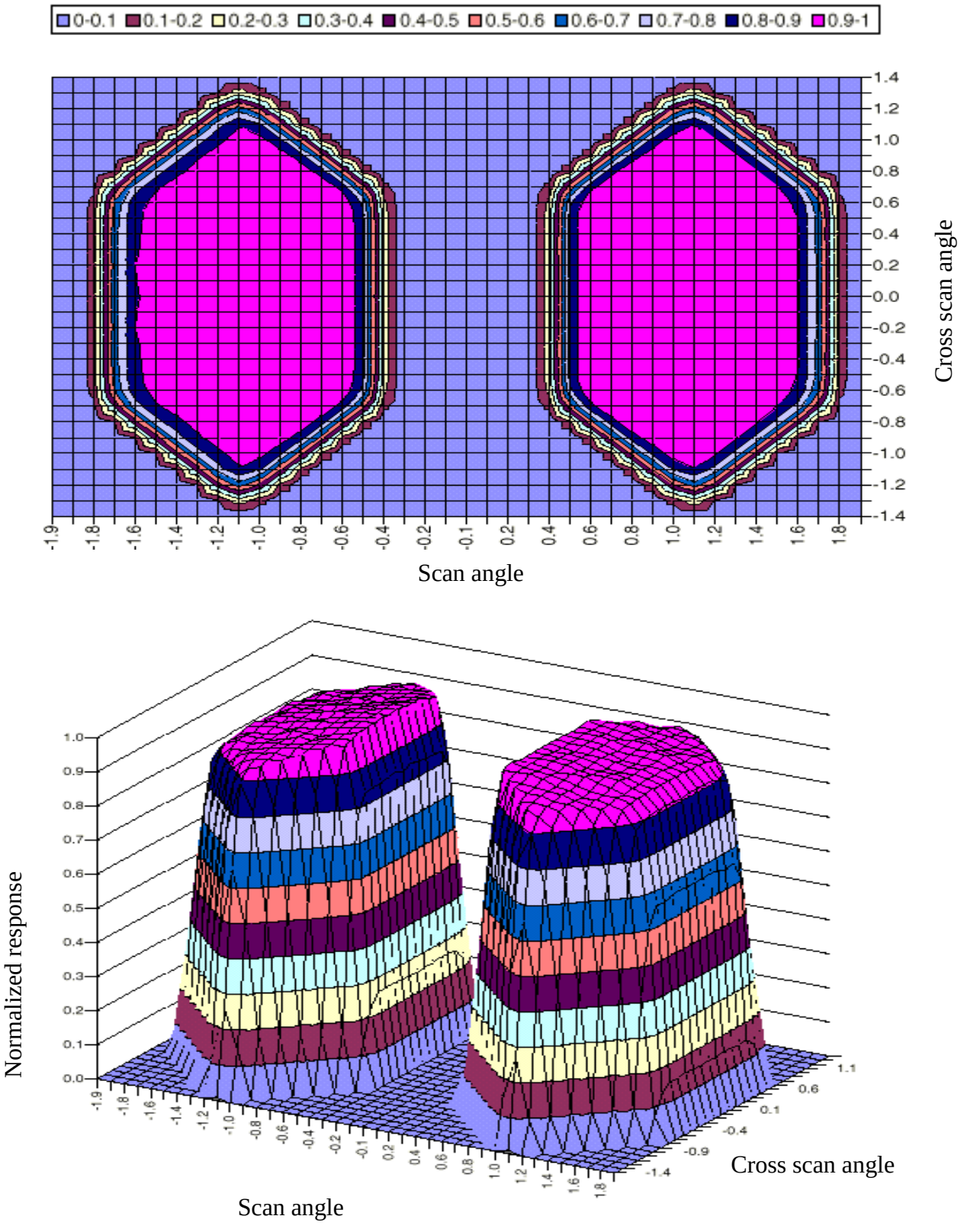

Figure 5.5 OPSF for the current CERES telescope with two (2) precision apertures.

5.2.2 Validation of results

The minimum blur circle found in the current study is 0.14 mm in diameter, comparing relatively well with the 0.122 mm diameter blur circle reported by TRW [Carman, 1993]. There is some discrepancy between the OPSF previously determined [Priestley, 1997], and the results of the current research effort in that the cutoff at the edges of the previous OPSF is not as steep as that of the results presented in this thesis. It is believed that this discrepancy occurred because the code used in the previous study did not model the telescope at best focus. Figure 5.6 compares results from the current and previous studies to those predicted by linear optics, and experimental data borrowed from Priestley [1997]. The curve predicted by linear optics was constructed by moving a blur circle of 0.14 mm in diameter across the detector and plotting the fraction of the blur circle area which would fall within the precision aperture. Figure 5.7 shows very good agreement between the results predicted by linear optics and current results, and reasonable agreement with experimental data.

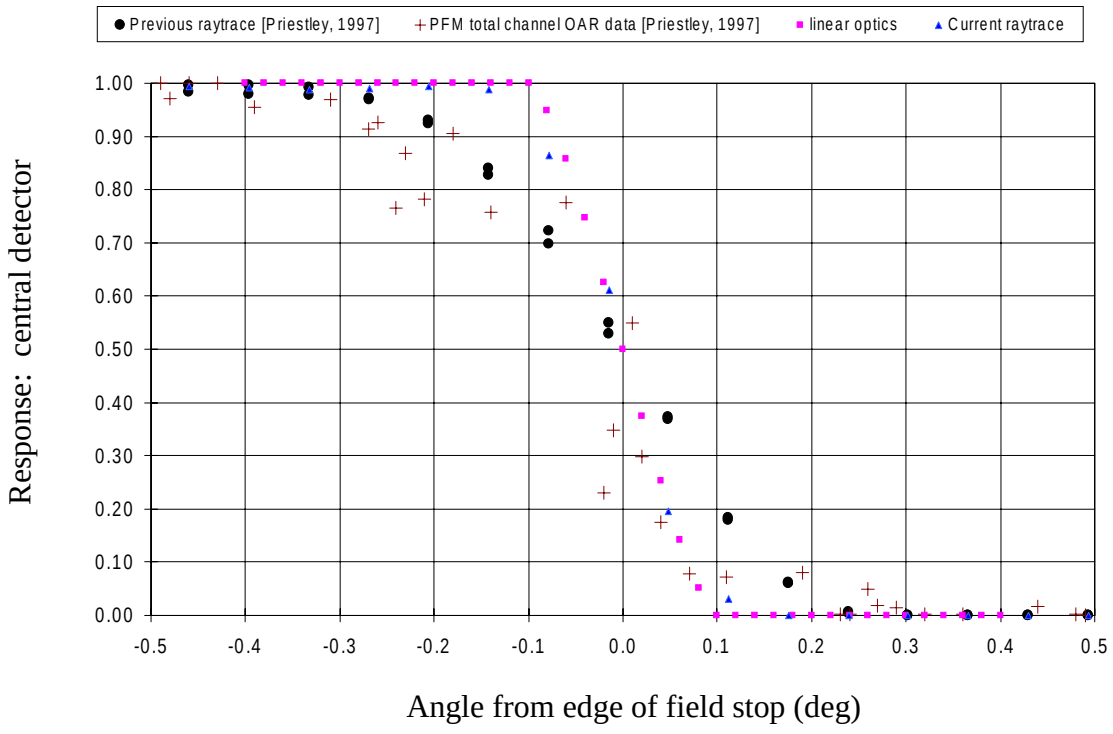

Figure 5.6 Comparison of current results with previous results, linear optics, and experimental data.

5.2.3 Conclusions: Use of existing CERES instrument with spherical mirrors

Figure 5.4 illustrates that the placement of five detectors in the current CERES instrument does not yield acceptable performance. A flat response across all detectors is desired, but a drop off in the response occurs at the two detectors furthest from the central axis. Note that the only modification to the current CERES telescope involved the removal of the primary mirror insert. Figure 5.5 shows that the placement of two detectors within the current CERES telescope does yield acceptable results, as the response is flat over the two detectors. It can be concluded that the capability of the current CERES instrument can be doubled by the addition of another detector in each telescope without sacrificing the quality of the OPSF. As previously mentioned, this modification would pose other challenges such as the possibility of optical cross-talk between channels.

5.3 Replacement of spherical mirrors with hyperbolic mirrors

5.3.1 Optical prescription for hyperbolic mirrors

In initial discussions of the potential next-generation design concept, PERSEPHONE, NASA engineers hypothesized that the replacement of spherical mirrors with hyperbolic mirrors within the same telescope could yield an instrument with good throughput over a significantly larger field of view, and with the same or smaller size blur circle. The basic parameters and layout of the current and potential future mirror systems are illustrated in Figure 5.7. The primary-to-secondary mirror spacing (vertex-to-vertex) is to be held the same, and only the curvatures and conic constants of the mirrors are to be changed. NASA engineers performed a preliminary study to determine the set of hyperbolic mirrors which met the required spacing and restricted mirror diameters that would yield the best performance. The constraints were entered into a commercial ray-trace code which iterates until finding the optimal combination resulting in the minimum blur circle. The recommended prescription is provided in Table 5.1.

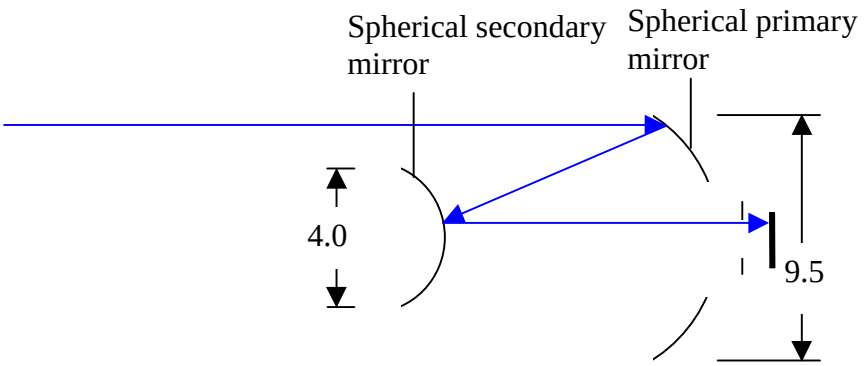

(a)

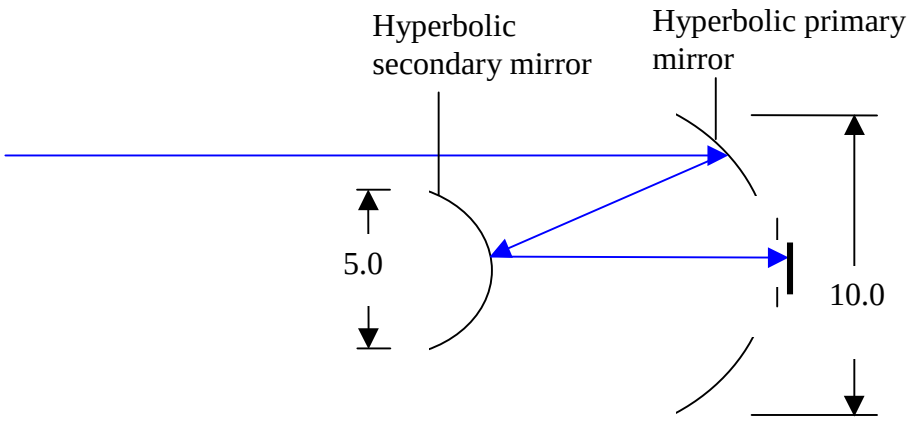

(b)

Figure 5.7 (a) Illustration of current CERES spherical mirrors (Modified Cassegrain), and (b) illustration of the new optical prescription with hyperbolic mirrors (Ritchey Crétian Cassegrain) (dimensions in mm).

Table 5.1 Optical prescription for hyperbolic mirrors.

	Primary Mirror	**Secondary Mirror**
r_v (vertex radius)	36.042 mm	32.284 mm
Max R (maximum mirror radius)	10.0 mm	5.0 mm
C.C. (conic constant)	-1.3329	-22.4729
Primary-to-secondary (vertex-to-vertex) spacing:	10.89 mm	
Primary vertex-to-detector plane spacing:	2.0 mm	

This combination of mirrors is said to yield blur circle sizes of 0.058 mm diameter on-axis, and 0.080 mm at 2.34 mm off-axis. The first objective in conducting this study was to use the new ray-trace tool to duplicate these results using only the mirrors. Upon successfully modeling this mirror combination, the next objective was to determine the Optical Point Spread Function of the hyperbolic mirrors and compare results with that obtained for the spherical mirrors.

In order to model the desired combination of mirrors, the parameters in Table 5.1 had to be converted into input required by the new MCRT environment. Details of this conversion are provided for two reasons: (1) in order to document the approach for future researchers, and (2) in order to clarify the appropriate use of several equations found in [Walkup, 1993], a reference commonly used by members of the Thermal Radiation Group.

5.3.2 Conversion of known parameters to required parameters

In order to specify hyperbolic mirrors using the new MCRT environment, the user must supply the parameters a, b, and c_h, parameters in the standard equation for a hyperboloid given by

$$\left(\frac{z}{c_h}\right)^2 - \left(\frac{y}{b}\right)^2 - \left(\frac{x}{a}\right)^2 = 1.0, \qquad (5.1)$$

where a=b for symmetrical optics. The parameters a and c_h are illustrated in Figure 5.8. Note that a is <u>not</u> the outer radius of the mirror slice, as stated by Walkup [1993].

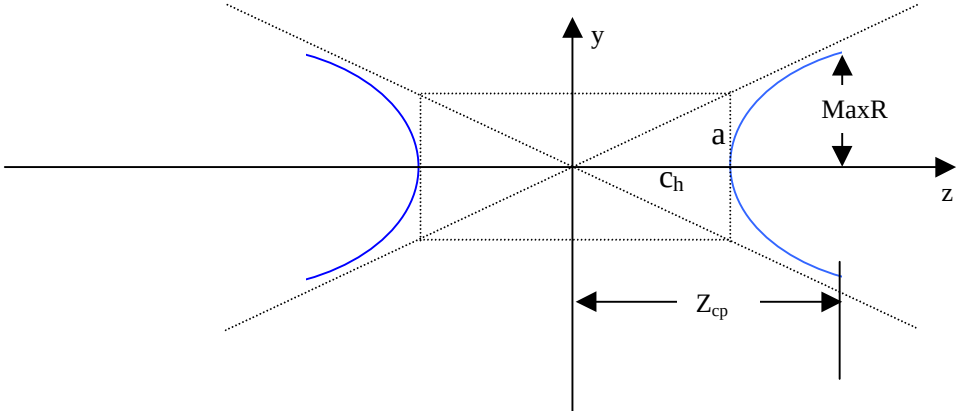

Figure 5.8 Illustration of parameters required for entry of hyperbolic mirrors into new MCRT environment.

Using the two expressions relating the parameters for a hyperboloid,

$$r_v = \frac{a^2}{c_h} \tag{5.2}$$

and

$$C.C. = -\frac{a^2 + c_h^2}{c_h^2}, \tag{5.3}$$

we have two equations and two unknowns. Therefore the parameters c_h and a can be determined. Because these are symmetrical optics, a = b. Finally, the dimension z_{cp}, is a required parameter, and could be found by substituting b = 0, a = Max R, and the value of c_h previously determined into equation 5.1. Using these parameters, the prescribed hyperbolic mirror combination was modeled with the new MCRT environment.

5.3.3 Results

The only results provided from the preliminary study conducted by NASA involved the size of the blur circle at several points on the focal plane. The central blur circle diameter was stated to be 0.058 mm when the vertex-to-vertex distance between mirrors, Δz, was 10.89. A similar result was obtained when the prescribed mirror combination was modeled using the new ray-trace tool, but the shape of this blur circle indicated that the mirrors are not at their best focus when Δz = 10.89 mm. Increasing Δz slightly resulted in a much smaller blur circle, as shown in Figure 5.9. The configuration yielding the smallest blur circle, where Δz = 10.93 mm, was used for the remainder of the studies conducted.

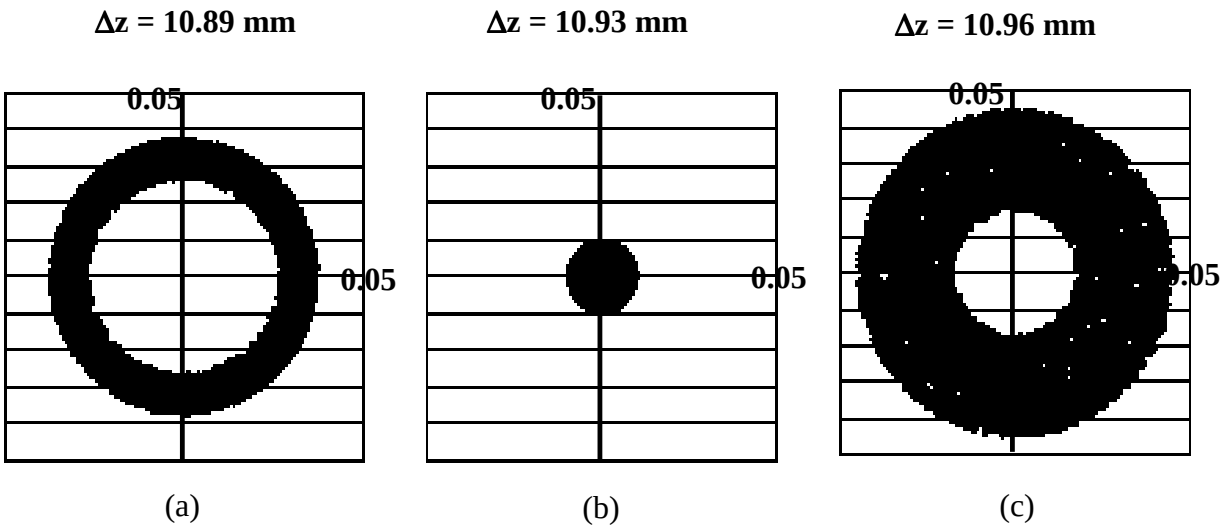

Figure 5.9 Illustration of blur circle minimization (where Δz indicates the distance between the primary and secondary mirrors) (dimensions in mm). (a) Defocused image, (b) image at best focus where the blur circle diameter is a minimum, and (c) defocused image.

The Optical Point Spread Function (OPSF) for the hyperbolic mirror combination was produced using the new MCRT environment. These results are shown in Figure 5.10 (b) compared to an OPSF generated for the spherical mirrors used in CERES, removed from the telescope (Figure 5.10 (a)). Only one half of the OPSFs are shown, as symmetry about the central axis is expected. Results presented in Figures 5.10 (a) and (b) serve to compare the performance of the spherical and hyperbolic mirror combinations alone, independent of the influence of the telescope geometry. Note that these OPSFs differ from those that would be obtained if the mirrors were placed within the telescope.

It is important to realize that the outer diameters of the hyperbolic mirrors are larger than those of the spherical mirrors; thus, some slight changes in the telescope would be required in order to use the recommended hyperbolic mirrors. NASA stated that this increase in diameter was a requirement for proper performance of the hyperbolic mirrors, and hyperbolic mirrors of the same diameters as the current spherical mirrors would not provide acceptable results.

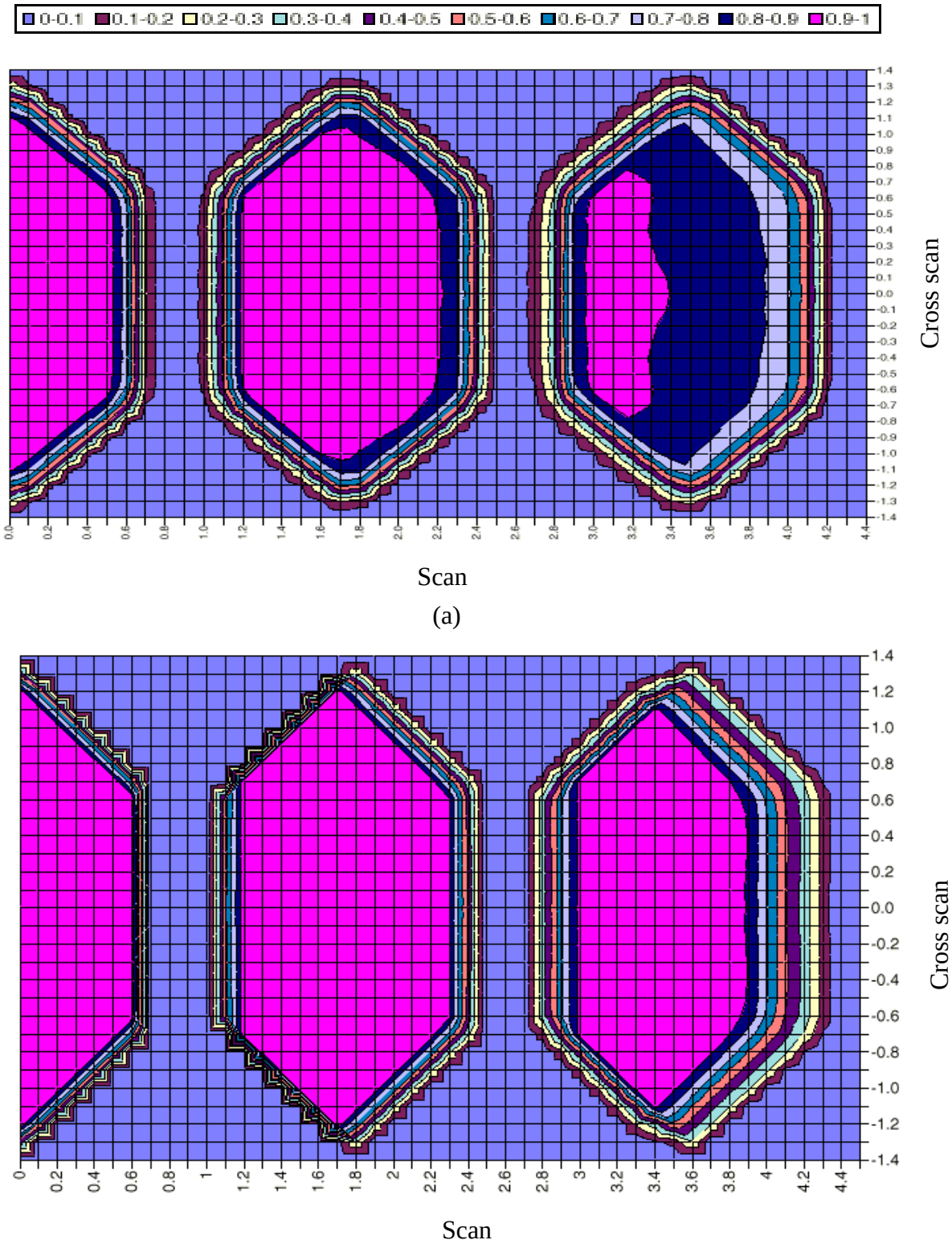

Figure 5.10 (a) OPSF of the current CERES spherical mirrors only, and
(b) OPSF of the prescribed hyperbolic mirrors only (profile view).

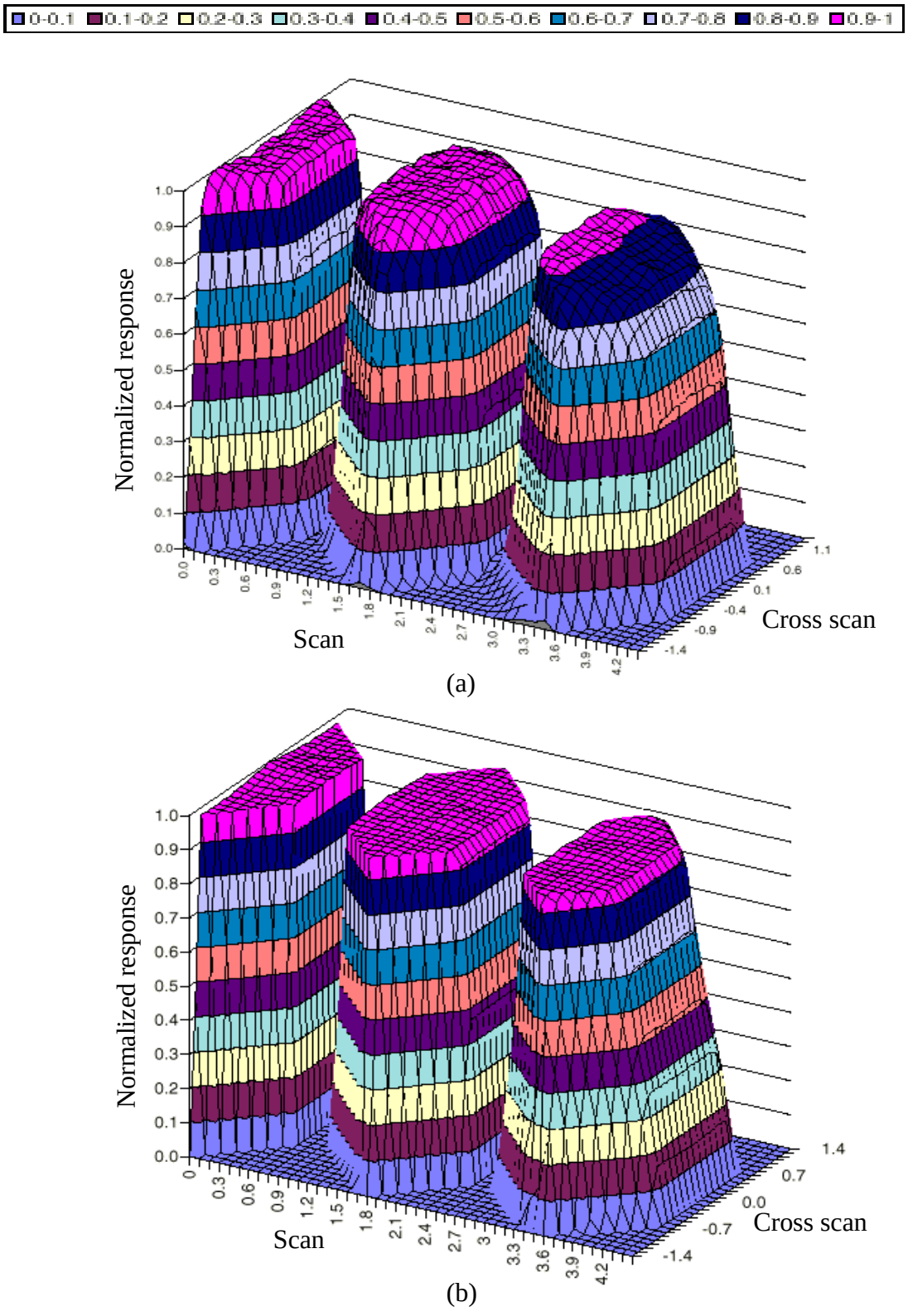

Figure 5.11 (a) OPSF of the current CERES spherical mirrors only, and
(b) OPSF of the prescribed hyperbolic mirrors only (relief view).

5.3.4 Conclusions: Hyperbolic mirrors

Figures 5.10 and 5.11 indicate that the hyperbolic mirrors provide the ability to produce a uniform flux over a larger area at the focal plane. Comparison of the OPSF of the spherical mirrors alone, shown in Figures 5.10 (a) and 5.11 (a), with that of the CERES telescope with the spherical mirrors (Figure 5.4) indicates that the drop-off in response is largely due to the manner in which radiation is transmitted through the telescope. (Here we are careful to distinguish between the full CERES telescope model; which includes baffles, secondary-mirror support struts, and other structural members; and an ideal optical system having the same prescription but consisting of only the two mirrors and the precision apertures). The drop-off due to the real telescope geometry would be expected in an instrument containing the hyperbolic mirrors as well, thus results **do not** show that a change in the mirrors will permit the use of five detectors in a given telescope. What is demonstrated is the improved performance of hyperbolic mirrors over spherical mirrors. Note, however that the current spherical mirror combination involves 45 percent obscuration while the hyperbolic mirror combination involves 55 percent obscuration. The result of such an increase in obscuration is less energy throughput and more problems with diffraction.

5.4 Potential future investigations

Future studies could involve the placement of the hyperbolic mirrors into an appropriately modified CERES telescope, and the determination of the resulting Optical Point Spread Function. The new MCRT environment could be used to study the effect of slight modifications of the interior telescope surfaces on the throughput to the detectors.

Another potential study could involve a different detector arrangement within the telescope. For example, instead of inserting extra detectors in a row, the detectors could be placed in some alternative arrangement which provides an optimal throughput to all detectors. One potential rearrangement for the insertion of four precision apertures is illustrated in Figure 5.12.

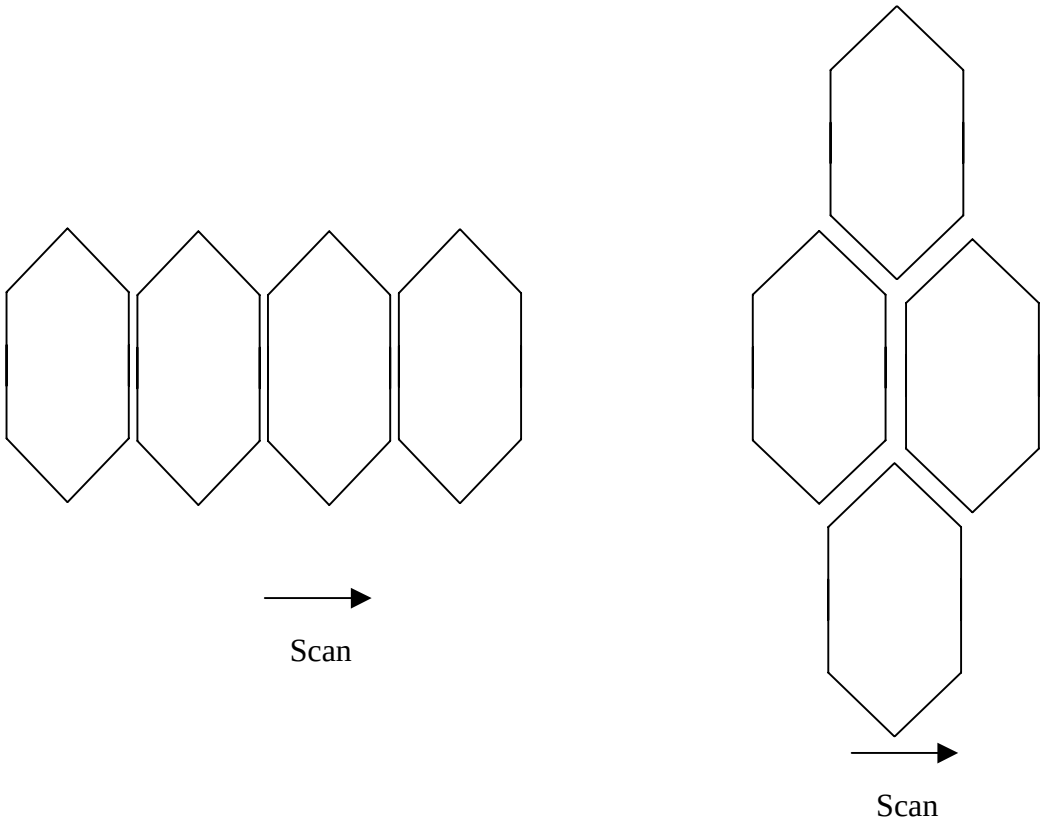

Figure 5.12 (a) Arrangement of precision apertures that has been considered, and (b) a potential arrangement of precision apertures for future study.